

## 2.5 Experimental Support for SHS Two-Scale Studies

In our effort to tie the experimental characteristics of heat sink to the theoretical scaled (VAT) description and simulation of semiconductor base-to-air heat sinks, we came to the process of coupling of two-scale modeling and experiment for heat sink design. Most past work focused on the upper scale performance characteristics resulting in many efforts to measure the bulk heat transport rate and in modeling of numerous morphologies (see, for example, Andrews and Fletcher (1996), Bejan and Morega, (1993); Bejan, (1995); Fabbri (1999); Jubran, Hamdan, and Abdualh (1993); Kim and Kim (1999); You and Chang (1997), etc.). In many cases, the experimental data were reduced to the homogeneous device effectiveness

$$E_{eff3} = \frac{Nu_w}{f_f Re_{por}^3}, \quad \text{¶}$$

where  $f_f$  is the momentum resistance in the volume, and  $Nu$ ,  $f_f$ , and  $Re$  are to be constructed using only one geometric parameter. The two scale, VAT upper scale governing equations applicable to this problem, contain four additional descriptive terms in the momentum equation (for 1D turbulent equation), seven terms in the fluid temperature equation, and five additional terms in the solid phase (reflecting heat transport through ribs, pins) temperature equations (Gratton et al. 1996; Travkin and Catton, 1999; Travkin et al., 2000).

At the present time, some basics known about developmental needs for VAT heat exchanger governing equations. Contrary to simulation numerical experiments, the physical experiment is usually much more restrictive in terms of the number of local experimental points that can be obtained. It is a problem to properly make local measurements and to relate the measurements within the volume of the heat exchange device to the results from simulations because the data point is a pint value and the simulation value is an average over a volume of finite size. In this modeling effort and experiment we attempt to deal with both using the two-scale approach.

## 2.6 Experimental Data Reduction Methods for Two-Phase Measurements in SHS

To analyze the performance characteristics we used the two of well known in heat exchangers industry parameters of convective heat transfer, which we would exploit in the detail.

1) – The heat transfer rate per unit volume per unit temperature difference when flux from below  $q_w$  is unknown

$$H_{r\infty} = \frac{S_{all} \bar{\alpha}_{all}}{\Omega} = \frac{(S_{wint} + S_{wb}) \bar{\alpha}_{all}}{\Omega} = S_w^* \bar{\alpha}_{all} = \text{¶} \frac{q_b^*}{(T_{wmax} - T_{in})} = Nu_{all} \frac{k_f}{d_{por}} S_w^* \text{¶} \left[ \frac{W}{m^3 K} \right] \text{¶}$$

where  $S_w^* = \frac{(S_{wint} + S_{wb})}{\Omega} \text{¶} \left[ \frac{1}{m} \right] \text{¶} \bar{\alpha}_{all} = \left( \frac{S_{wint} \bar{\alpha}_{int} + S_{wb} \bar{\alpha}_b}{(S_{wint} + S_{wb})} \right) \text{¶} \left[ \frac{W}{m^2 K} \right] \text{¶}$  are the overall specific surface and the heat transfer coefficient. When the heat flux  $q_w$  which is entering from below is known, then the heat transfer rate is

$$H_{rwc} = S_b^* \frac{q_w}{(T_{wmax} - T_{in})} = Nu_w \frac{k_f}{d_{por}} S_b^* \text{¶} Nu_w = \frac{q_w d_{por}}{(T_{wmax} - T_{in}) k_f} \text{¶} \alpha_w^* = \frac{q_w}{(T_{wmax} - T_{in})} \text{¶} S_b^* = S_b / \Omega. \text{¶}$$

The characteristic of pumping power per unit volume

$P_p = \frac{P}{\Omega} \left[ \frac{W}{m^3} \right] = \frac{\dot{m}_c \Delta p}{\rho_f \Omega} \llcorner = f_f \langle m_{yz} \rangle \left( \frac{S_w}{\langle m \rangle} \right) \frac{\rho_f \tilde{U}_b^3}{2} \llcorner \left[ \frac{W}{m^3} \right] \llcorner$  which was used written in the VAT notations, is the important one to assess the general level of performance of the heat exchange device. If the two parameters above relate one to another then an effectiveness parameter

$E_{effl} = H_{rwc} / P_p = \left[ Nu_w \left( 32 \frac{S_b^* \langle m \rangle^3}{\langle m_{yz} \rangle S_w^3} \right) \frac{k_f \rho_f^2}{\mu^3} \right] / [f_f Re_{por}^3] \llcorner \left[ \frac{1}{K} \right] \llcorner$  is appeared for the situation when heat flux from the semiconductor device is known.

In the semiconductor heat sink there are the two phase participating in the heat rejection process – the fluid (air) and the solid one. The second is no less important as the first phase. Nevertheless, the most (if not the only) used parameters are all calculate the fluid phase heat transfer distribution. We used to introduce the second phase heat transfer parameters, as the heat transfer rate and other. For example, for the round pin fins we determined the solid phase lower scale homogeneous parameter as

$H_{rsc} = \frac{S_{ws} q_s}{\Omega (T_{wmax} - T_{in})} = \left( -k_s \frac{\partial T_s}{\partial z} \right) \frac{(\pi R_{pin}^2) n_{pins}}{L_x L_y L_z (T_{wmax} - T_{in})} \llcorner$  which is the parameter calculated with the help of experimentally obtained data.

### 2.7 Analysis of Simulation and Experiments Using Homogeneous and Heterogeneous Two-Scale Approaches

The heat transfer rate  $H_{rwc}$  and the effectiveness number  $E_{effl}$  has been explicitly used for comparison of our four sink samples - three samples with staggered pin fins and one sample with longitudinal fins - Figures 3-4. The low-speed wind tunnel with an open circuit design is composed of the following sections: (a) an inlet section that includes flow conditioners like flow straighteners and turbulence control screens; (b) a contraction cone or nozzle that accelerates the flow; (c) test section that contains the model to investigate; (d) a diffuser that reduces the air speed with as little energy loss as possible; (e) a fan driven by a split capacitor motor that is controlled by an AC-V fan speed control. The wind tunnel is operated in the suction mode; ie, the fan sucks atmospheric air through the fin assembly and the test section via the bell-mouthed entrance section, with the fan and motor assembly on the exhaust side of the system.

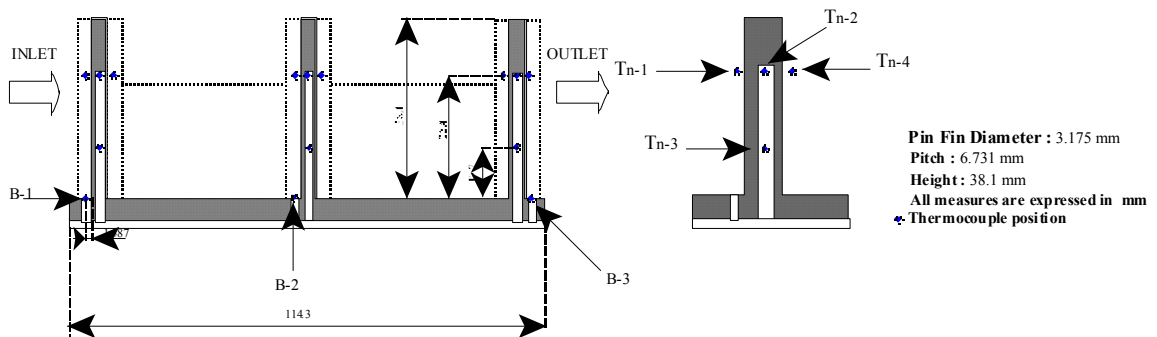


Figure 3 Thermocouple locations inside and outside of pin fins

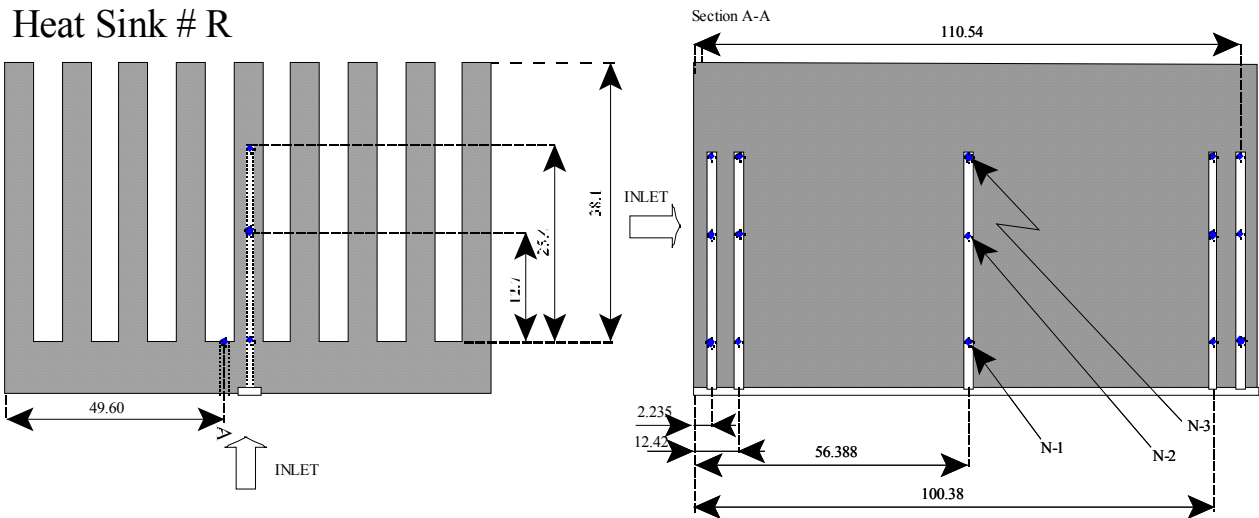


Figure 4 Longitudinal heat sink #R cross-sections and thermocouple locations

The overall pressure drop through the heat sink is obtained via two static-pressure taps located at the bottom of the test section. A standard differential pressure gage is used. In order to evaluate the velocity profile and the flow rate, velocity measurements were carried out using an air velocity transducer of cylindrical shape, which is inserted from the side walls of the test section Figure 3. Measurements were taken upstream and downstream of the surface to be tested.

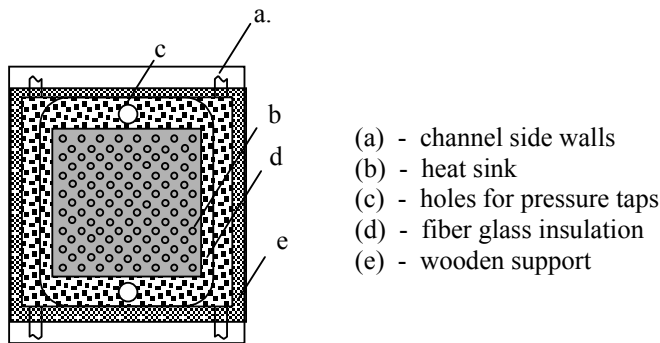


Figure 5 Top view of pin fin heat sink fixture

The heat generating source plays an important role in the design of the experimental setup. It serves as a heat source in order to investigate the heat transfer to the environment and pressure loss characteristics of the augmented surface. Three cartridge heaters rated

250 W, each were inserted into a copper block with the same area as the heat sinks (114.3mm by 114.3mm) and a thickness of 25.4 mm. An estimation of the losses through the sides of the wooden box using thermocouples located on each side of the wooden box. The heat sink to be tested is mounted on the copper block.

Under all the test conditions employed, more than 98% of the heat generated in the copper block passed, through the finned heat sinks, to the air in the wind tunnel duct. The whole heater box is such that it can be taken apart and assembled easily in few minutes.

Temperatures of the copper block were taken by an array of three K thermocouples; temperature profile of the heat sink base was provided by an array of three J thermocouples located along the air flow direction. To apply the corresponding VAT simulation techniques, temperatures along the pin fins were taken. For each of three pin fin heat sinks along the flow direction, temperatures forward and backward were measured. Furthermore, the same pin fins were drilled to allow the collocation of two wires in order to measure the pin fin temperature at 1/3 and 2/3 of its height. The same technique was used for longitudinal fins sink - Figure 4.

Three narrow channels were grooved at the bottom of the aluminum heat sinks in order to guide the thermocouples out of the heat sink without affecting the surface contact between the aluminum heat sink and the copper block. The narrow channel, where the thermocouple wires were inserted, were then filled with high-conductivity thermal paste. This solution does not affect the air flow pattern into the heat sink. J thermocouples of 0.005" in diameter were used. The inlet and the outlet air stream temperatures in the wind tunnel duct were measured using a thermocouple located at the tip of the anemometer probe. Mapping the velocity profile a map of the temperature distribution is also done. Every thermocouple was calibrated before being installed.

The heat dissipating enhanced surfaces of pin fin samples are made of aluminum with a conductivity of 225 [W/m K], while the longitudinal fin sink has aluminum conductivity 204 [W/m K]. Each of the three pin fin heat sinks had constant fin height 0.0381m, constant fin diameter 0.00318m, but the pitch was varied. All the three pin fin heat sinks tested had a staggered pin fin layout.

The series of experiments were initiated with the fin array #1, corresponding to a  $P/d = 3$ . The all heat sinks were tested with no-bypass set up. At steady state conditions, pressure drop and temperature were recorded. For the same input power, four different velocities were tested. Every time the steady state was assured before data was collected. The procedure was then repeated for input powers close to values of 50, 125 and 222 [W]. For every heat sink 12 data points have been taken. The different parameters and their values for pin fin sinks studied

in this investigation are given in Table 1.

PARAMETER	VALUE
Diameter of pin fins	0.3175 cm
Height of pin fins	3.81 cm
Pitch h.s. staggered array #1	0.9525 cm
Pitch h.s. staggered array #2	0.71425 cm
Pitch h.s. staggered array #3	0.47625 cm
Longitudinal fins sink length	112.78 cm
Longitudinal fins sink height of fins	3.81 cm
Heat input, $Q_{in}$	50, 125, 222 W
By-pass	No
$Re_{por}$	500 ÷ 20000

The repeatability of the experiment was demonstrated by repeat testing. The samples studied show a consistent pattern of declining friction factor  $f_f$  with increasing porous media Reynolds number  $Re_{por}$ , see Figure 6. The range of measured Fanning friction factor  $0.15 < f_f < 0.8$  in Figure 6 compares well with other well known correlations for Fanning

friction factor in this range of Reynolds number defined using the VAT formulation (Travkin and Catton, 1998). Travkin and Catton (1998) and Travkin et al. (1999) recalculated a number of results found in the literature using the VAT based formulae, see Figure 7, and found substantial differences for this kind of combined heat transfer in comparison to internal media

heat transfer coefficient correlations. Also, the heat transfer rate,  $H_r$  (Figure 8) and the Nusselt number (Figure 7) curves, for all experiments ( $4 \times 12 = 48$ ), are different.

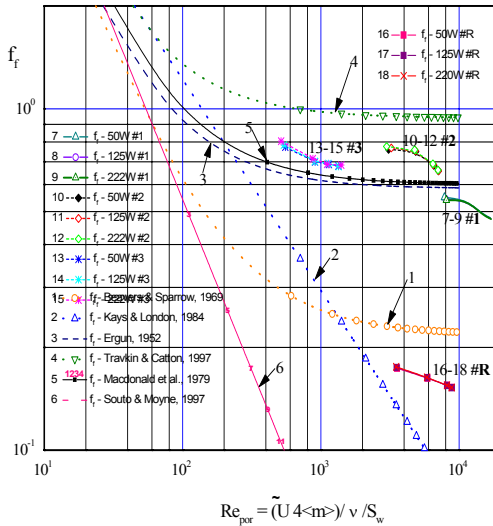


Figure 6 Fanning friction factor  $f_f$  (bulk flow resistance in SVAT for different media morphologies, materials and scales used), reduced based on VAT scale transformations in experiments by: 1) Beavers and Sparrow (1969); 2) Kays and London (1984); 3) Ergun (1952); 4) (Travkin and Catton, 1997); 5) Macdonald et al. (1979); 6) Souto and Moyne (1997); 7-9) sink #1; 10-12) sink #2; 13-15) sink #3; 16-18) longitudinal fins sink.

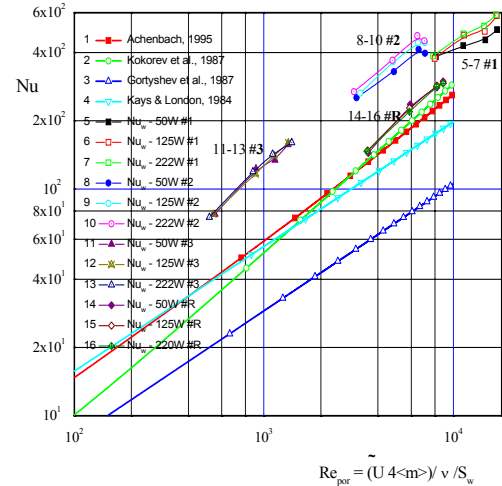


Figure 7: Internal effective heat transfer coefficient in porous media, reduced based on VAT scale transformations in experiments and analysis by: 1) Achenbach (1995); 2) Kokorev et al. (1987); 3) Gortyshov et al. (1987); 4) Kays and London (1984); 5-7) sink #1; 8-10) sink #2; 11-13) sink #3; 14-16) sink #R

The Figure 9 presents measurements of the effectiveness based on the heterogeneous formulation of  $E_{eff1}$  and Figure 10 shows its counterpart based on the conventional homogeneous formulation. The conclusion drawn from these figures is that the three investigated versions of the same morphology (pin fins) have different effectiveness in different ranges of momentum intensity ( $Re_{por}$ ). The primary difference between the two figures is the scale. The effectiveness defined using the VAT formulation, however, is much richer in that it contains the parameter dependence of lower scale on upper scale, which the homogeneous formulation cannot.

Compare the two kinds morphology of semiconductor heat sink it is possible to make preliminary observation based on the Figures 6-9 that the third pin fins sample with more dense packing of fins is the most effective among all four.

This conclusion is not available to reach if one could have the homogeneous characteristics of Figures 7, 10 because they contradict one to another – Figure 7 suggests that the best among these three samples is the sample #1. Meanwhile, compare effectiveness in Figure 10 we can see that the most effective is the sample #3. In our application the most

important is the characteristic of how much energy can be transported outside of the heat sink, but not the amount of energy used for this.

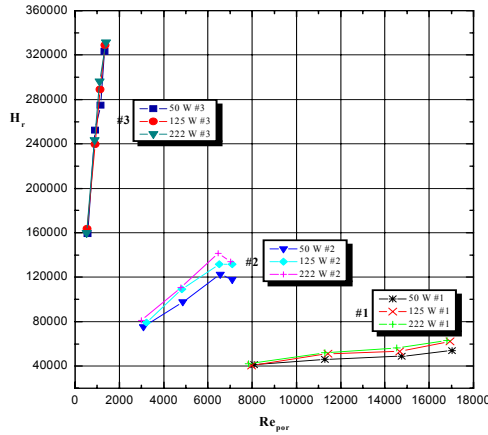


Figure 8 Homogeneous bulk one-phase heat transfer rate  $H_r(Re_{por})$  for three pin fin heat sinks

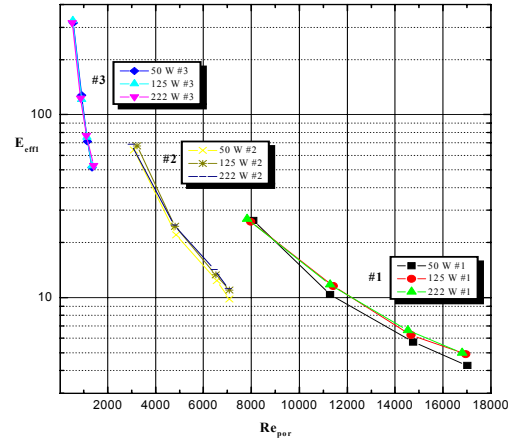


Figure 9 Heterogeneous bulk Effectiveness  $E_{effl}(Re_{por})$  for three pin fin heat sinks

Based on these reasoning's designer can compromise in a favor of heat sink #1, which is the least effective, but can withdraw the largest amount of heat in accordance with  $Nu_w$  in Figure 7. This decision can be justified only when the volume of device is not an issue, which usually untrue.

Otherwise, comparing curves in Figure 8 for the heat transfer rate per unit volume designer would see that the sample #1 is not only the least effective, but can dissipate the smallest amount of heat per unit volume of heat exchanger. That might be the decisive observation.

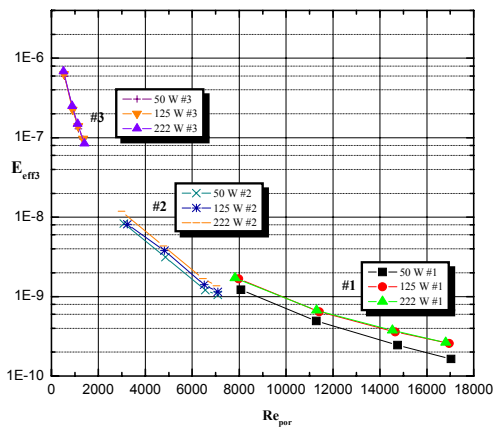


Figure 10 Homogeneous Effectiveness  $E_{eff3}(Re_{por})$  for three pin fin heat sinks

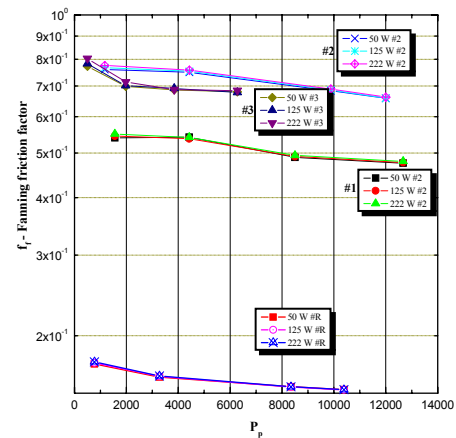


Figure 11 Fanning friction factor  $f_f(P_p)$ , momentum resistance for all four types of heat sin

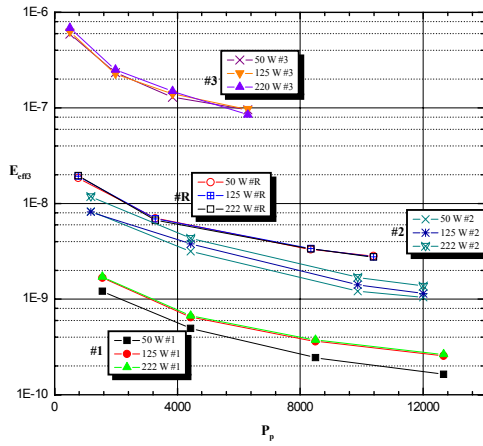


Figure 12 Homogeneous effectiveness parameter  $E_{eff3}(P_p)$  for all four types of heat sinks

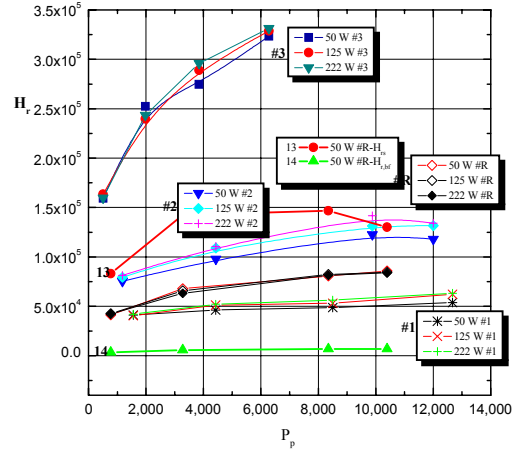
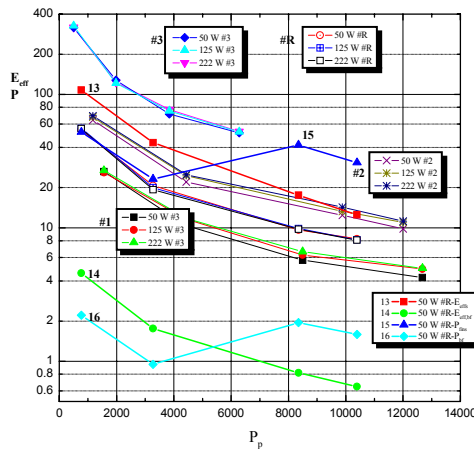


Figure 13 One-phase bulk heat transfer rate  $H_r(P_p)$  for all four types of sinks, solid phase heat transfer rate  $H_{rs}(P_p)$  and bottom surface (minus fins occupied area) fluid phase heat transfer rate  $H_{r,bf}(P_p)$  in experiments with heat sink #R

Figure 14 One-phase bulk heterogeneous effectiveness  $E_{eff1}(P_p)$  for four types of heat sinks as well as solid phase effectiveness  $E_{effs}(P_p)$  and bottom surface (minus fins occupied area) fluid effectiveness  $E_{eff,bf}(P_p)$  and dissipated through fins  $P_{fins}(P_p)$  and bottom surface  $P_{bf}(P_p)$  amount of heat in experiments with heat sink #R

Also, the homogeneous effectiveness formula curves in Figure 10 look like they are ready to be used for integration of all three pin fin sinks effectiveness data via approximation of the data by one curve. This could be inappropriate data reduction move according to heterogeneous scaling results of Figure 9. There are still insufficiencies in the applied above performance characteristics and some of them would be improved further.

Further, as one would note that the primary assigning parameter in experiments is the pumping power per unit volume  $P_p$  which was used to set up the comparable conditions for different sinks and regimes. This parameter as independent variable is much better ground for comparison of different devices with different conditions as seen in Figures 11-14 where all the sinks performance results are exposed more obviously for deriving conclusions. For example, the homogeneous effectiveness  $E_{eff3}$  curves for pin fin sink #2 and longitudinal sink #R in Figure 12 are located as the sink #R is slightly better performer than sink #2. But observation of Figures 13,14 makes clear that the sink #2 is better in this range of  $P_p$  and more of that, the sink #2 probably reaching its maximum of performance approximately at  $P_p = 10500$ . There are the phase based definitions of the effectiveness parameters of solid phase  $E_{effs} = H_{rs}/P_p$  and the bottom flat surface fluid phase effectiveness  $E_{eff,bf} = H_{r,bf}/P_p$  - Figures

13,14. These parameters are more accurate in the power balance calculations as we calculated and are directly involved in the VAT based bulk mathematical governing equations modeling in a simple way as is the heat sink problem in the flat channel.

Meanwhile, the more profound and accurate studies of heat sink performance optimization revealed in a more obvious way that the sink's heat exchange rate or effectiveness maximization is the real multidimensional problem, but not only a dependency on  $Re_{por}$ ,  $f_f$  or heat exchange coefficients (Travkin et al., 2000, 2001).

### *2.8 Phase Separated Simulation and Analysis of Experimental Data Homogeneous Characteristics Performance*

The more thorough analysis of performance characteristics of two measured samples of SHS surfaced the few very important conclusions.

The primary goal for decomposition of the entire set of the SHS performance characteristics was to get more information and understanding of how unequal is in reality the heat exchange in different parts of the SHS. The complete picture and data reduced were obtained from the detailed two phase numerical simulation and will be discussed later. Nevertheless, the physical modeling - experiment is provided to cast a light on the problem by comparing the different modeling approaches.

While considering the problem of experimental set-ups and experimental data reduction for the two-scale semiconductor heat sink, a number of new criteria for momentum and heat transport were derived to connect the local and overall (as temperature in inlet and outlet, etc.) characteristics to the parameters of VAT scaled models. The reason for heterogeneous parameter usage is shown while accomplishing the analysis of the experimental results for heat sink performance - it yields a better, more exact description of the influence of the media and both phase characteristics on transport values.

These parameters are so specific that they allow one to distinguish the input of any mechanism or mode of heat transfer occurring in the device. The heat transfer device is presented as two-scale local- non-local heterogeneous heat exchanger with controls on both scales. For example, the heat transfer rates and effectiveness formulated for both phases, which improve the energy balance assessment.

We have outlined the consequences of the experimental procedures and design, because the larger number of influencing phenomena make possible the larger number of choices in optimization of performance or in increasing the heat exchange rate to its possible highest level. The latter is the goal of preference in cooling of semiconductor devices. Experimental results were simulated using non-local VAT model and also compared to a number of works in the area of heat sink design and simulation:

a) There is the one result which came out of this method and which should be considered as the one of a good value - is that the separate phase heat exchange fluxes and parameters are not equal to those averaged over the bottom surface heat flux and heat transfer rate parameter  $H_{rwc}$ .

b) It is worth to note here that in all the simulation procedures pertinent to the phase-separate heat transfer assessments (as well as to one phase SHS performance assessment) there is no need for the heat transfer coefficient on any surface to be considered or calculated, but for the rudiment resistance assessment.

Another important conclusion is that the heat performance experiment was disclosed from the unusual side allowing making some assessment about its value. Above made analysis for the pin fins SHS suggests that the power amount is overcalculated in both submedia - for the pin fins heat transfer rate and for the wetted bottom surface heat transfer rate. But the reasons for that are different:

1) in the case of pin fins - the reason for too big energy amount is - the heat flux in the pins is taken well above the value of it as it is being in reality;

2) in the case of the bottom surface in the pin fins SHS - the reason for the too large heat dissipated is that - the averaged experimental flux  $q_w=3794.408$  is also too big - it is averaged over the entire bottom surface including the relatively higher flux via the pins and unjustifiable and unrealistically high for the wetted part of the bottom surface.

That is the one more reason for the better designed experiment - this kind of experiments we did so far are not fit to the standards of the two-scale studies. We will discuss few of the implications in the following sections.

For the "R" longitudinal fins SHS:

1) We achieved good heat transfer rates for all three parameters used, for example, in the data reduction for sink with  $P_p=3276.78$  [W/m<sup>3</sup>] as - the heat transfer rate homogeneous overall  $H_{rwc}=11099.$ , [W/m<sup>3</sup>K], via the bottom surface heat transfer rate  $H_{rbf}=895.84$ , [W/m<sup>3</sup>K], and even via the fins heat transfer rate  $H_{rs}=11878.$ , [W/m<sup>3</sup>K];

2) We achieved much better energy balance for this SHS: in the fins  $-P_{fins,diss}=51.81$  [W]; at the bottom surface energy balance  $P_{bf,diss}=3.91$  [W], and even the overall device homogeneous energy balance  $P_{bulk,diss}=48.41$  [W], is corresponding to the previous two, when using appropriate values of temperatures. Summarizing table shows these and other parameters

	$P_p \left[ \frac{W}{m^3} \right]$	$H_{rs} \left[ \frac{W}{m^3 K} \right]$	$H_{rbf} \left[ \frac{W}{m^3 K} \right]$	$H_{rwc} \left[ \frac{W}{m^3 K} \right]$	$E_{effs} \left[ \frac{1}{K} \right]$
Pin fins	501.8852	14,452	440.8	9,146	28.795
"R"	769.37	6,929	610.4	6786.6	9.0
"R"	3276.785	11878.63	895.84	11099.58	3.63

$E_{eff,bf} \left[ \frac{1}{K} \right]$	$(E_{effs} + E_{eff,bf}) \left[ \frac{1}{K} \right]$	$E_{eff,wc} \left[ \frac{1}{K} \right]$
0.878	29.673	18.22
0.7934	9.793	8.82
0.273	3.903	3.387

There are still the uncertainties in this kind of data collection and reduction for the SHS and we had addressed these issues in the further studies. Some of the inconsistencies and inaccuracies in assessments are based or have origins in:

1) The methods of data collection for the temperatures in the fins and on the bottom surface;

2) The magnitudes of particular interest - the heat fluxes are not assessed at the bottom surface and are not connected to the VAT variables.

3) The amount of data measured is not sufficient for the purposes of assessment of surface or fluctuation functions in the subvolumes and over the surfaces.

4) The balances of energies and heat transfer rates are not good enough for the satisfactory grade judgment.

5) The parameters of homogeneous heat transfer assessments - those as the heat transfer rate  $H_{rwc}$ , for example, and the effectiveness  $E_{effs} = H_{rs} / P_p$  are not related to the VAT upper scale heat transport statements, and as such have low values in helping to evaluate the process and to find the better design.

### *2.9 Methods of Design of the SHS Using the Two-Scale Approach*

For the models and differential equations describing HE's to be useful, the additional integral and integro-differential terms need to be addressed in a systematic way. VAT has the unique ability to enable the combination of direct general physical and mathematical problem statement analysis with the convenience of segmented analysis usually employed in HE design. A segmented approach is a method where overall physical process or group of phenomena are divided into selected subprocesses or phenomena that are interconnected each to others by an adopted chain or set of dependencies. A few of the obvious steps that need to be taken are including:

- 1) model what increases the heat transfer rate;
- 2) model what decreases of flow resistance (pressure drop);
- 3) combining the transport ( thermal / mass transfer) analysis and structural analysis (spacial) and design;
- 4) find the minimum volume ( the combination of parameters yielding a minimum weight HE);
- 5) include nonlinear conditions and nonlinear physical characteristics into analysis and design procedures.

The power and convenience of this method is clear, but its credibility is greatly undermined by variability and freedom of choice in selection of subportions of the whole system or process. The greatest weakness is that the whole process of phenomena described by voluntarily assigned set of rules for the description of each segment is sometimes done without serious consideration of implications followed by such segmentation. Strict physical analysis and consideration of the consequences of segmentation is not possible without a strict formulation of the problem which the VAT based modeling supplies. Structural optimization of a plate HE, for example, using the VAT approach might consist of the following steps:

- 1) Optimization of the number of plates, plate spacing and fin spacing;
- 2) Optimization of the fin shape;
- 3) Simultaneous optimization of multiple mathematical statements.

This approach allows also consideration and description of hydraulically and thermally developing processes by representing them through the distributed partial differential systems.

- 1) For the range of a Temperature of an Incoming Air in SHS.
- 2) For the range of a Power to be Dissipated in SHS.
- 3) For the range of Air Velocity Used (pressure drop) for the particular Class of Assigned Morphologies of the SHS.

4) Nonlinearities in the Phenomena Causing the Additional Spread (distribution) of the Optimum "Surface" to an Optimum Volume.

The enhancement of a heat transport process is stated mathematically in a way that the lower scale conventional pin heat transport enhancement and the performance of the total device are incorporated for optimization. The problem is addressed in three steps: 1) solution of a two-temperature problem with inclusion of experimental data correlations, 2) statistical design of experiments (simulating the problem) for problems with many optimization parameters, and 3) optimization of 2D heterogeneous volumetric heat removal by conduction and convective exchange. The analysis distinguishes certain classes of distributed parameter optimization statements whose solutions determine global "in-class" upper limits of heat enhancement (for a given set of physical assumptions).